

CD-g-CS nanoparticles for enhanced antibiotic treatment of *Staphylococcus xylosus* infection

Si-Di Zheng,^{1,2,†} Zhi-Yun Zhang,^{1,2,†} Jin-Xin Ma,^{1,2} Qian-Wei Qu,^{1,2} Bello-Onaghise God'spowe,^{1,2} Yue Qin,^{1,2} Xue-Ying Chen,^{1,2} LU Li,³ Dong-Fang Zhou,⁴ Wen-Ya Ding^{2,5,*} and Yan-Hua Li^{1,2,**}

¹College of Veterinary Medicine, Northeast Agricultural University, Harbin, Heilongjiang, 150030, China.

²Heilongjiang Key Laboratory for Animal Disease Control and Pharmaceutical Development, Harbin, Heilongjiang, 150030, China.

³College of Life Science, Northeast Agricultural University, Harbin, Heilongjiang, 150030, China.

⁴School of Pharmaceutical Sciences, Southern Medical University, Guangzhou, 510515, China.

⁵School of Pharmacy, Guangxi University of Chinese Medicine, Nanning, 530200, China.

Summary

***Staphylococcus xylosus* (*S. xylosus*)-induced cow mastitis is an extremely serious clinical problem. However, antibiotic therapy does not successfully treat *S. xylosus* infection because these bacteria possess a strong biofilm formation ability, which significantly reduces the efficacy of antibiotic treatments. In this study, we developed ceftiofur-loaded chitosan grafted with β -cyclodextrins (CD-g-CS) nanoparticles (CT-NPs) using host-guest interaction. These positively charged nanoparticles improved bacterial internalization, thereby significantly improving the effectiveness of antibacterial treatments for planktonic *S. xylosus*. Moreover, CT-NPs effectively inhibited biofilm formation and eradicated mature biofilms. After mammary injection in a murine model of *S. xylosus*-induced mastitis, CT-NPs significantly reduced bacterial burden and alleviated inflammation, thereby achieving optimized therapeutic efficiency for *S. xylosus* infection. In conclusion, this treatment strategy could improve the efficiency of**

antibiotic therapeutics and shows great potential in the treatment of *S. xylosus* infections.

Introduction

Staphylococcus xylosus (*S. xylosus*) is an important, conditionally pathogenic bacterium associated with cow mastitis (Akhaddar *et al.*, 2010; Rumi *et al.*, 2013; Tan *et al.*, 2014). In recent years, instances of cow mastitis caused by *S. xylosus* have been increasing and have seriously threatened the dairy industry (Osman *et al.*, 2016). Antibiotics are currently used as common therapeutics for *S. xylosus* infection. Unfortunately, the therapeutic efficacy of conventional antibiotics is unsatisfactory because *S. xylosus* possesses a strong ability to form biofilms (Xu *et al.*, 2017). Biofilms are complex, three-dimensional structures composed of cell aggregates encased within a self-produced matrix of extracellular polymeric substances (EPS) that adhere to each other and a surface. Compacted EPS can act as a barrier to protect bacteria from antimicrobial agents (Kouidhi *et al.*, 2015; Flemming *et al.*, 2016; Makovcova *et al.*, 2017), making bacteria in biofilms 10–1000 times more resistant to conventional antibiotics than non-biofilm forming bacteria (Planchon *et al.*, 2006; Xu *et al.*, 2017). Accordingly, the therapeutic efficacy of traditional antibiotic treatments on *S. xylosus* is reduced by the formation of biofilms. As a result, it is difficult to eradicate *S. xylosus* infection using antibiotics, despite prolonged treatment duration (Parsek and Singh, 2003; Planchon *et al.*, 2006).

Ceftiofur (CT), a third-generation cephalosporin, is widely used for treating cow mastitis due to its excellent antibacterial activity and lack of significant toxic side effects (Wang *et al.*, 2018; Locatelli *et al.*, 2019; Flores-Orozco *et al.*, 2020). However, the formation of *S. xylosus* biofilms compromises its effectiveness. The antibacterial mechanism of CT is based on the inhibition of peptidoglycan synthesis by binding to intracellular, penicillin-binding proteins (Helbling *et al.*, 2020). This indicates that its antibacterial efficacy is closely correlated to its concentration in the targeted bacteria. In clinical practice, the typical commercial formulation used is ceftiofur sodium (CTS) injection. Sadly, the short retention time of CTS results in a lower CTS concentration in the targeted bacteria between administration intervals,

Received 22 November, 2020; revised 2 June, 2021; accepted 6 June, 2021.

For correspondence. *E-mail dingwenya306@163.com; Tel. +86 0771 4953513. **E-mail liyanhua@neau.edu.cn; Tel. +86 0451 55191881; Fax. +86 0451 55191881.

[†]These two authors contributed equally.

Microbial Biotechnology (2022) 15(2), 535–547
doi:10.1111/1751-7915.13870

© 2021 The Authors. *Microbial Biotechnology* published by Society for Applied Microbiology and John Wiley & Sons Ltd.

This is an open access article under the terms of the Creative Commons Attribution-NonCommercial License, which permits use, distribution and reproduction in any medium, provided the original work is properly cited and is not used for commercial purposes.

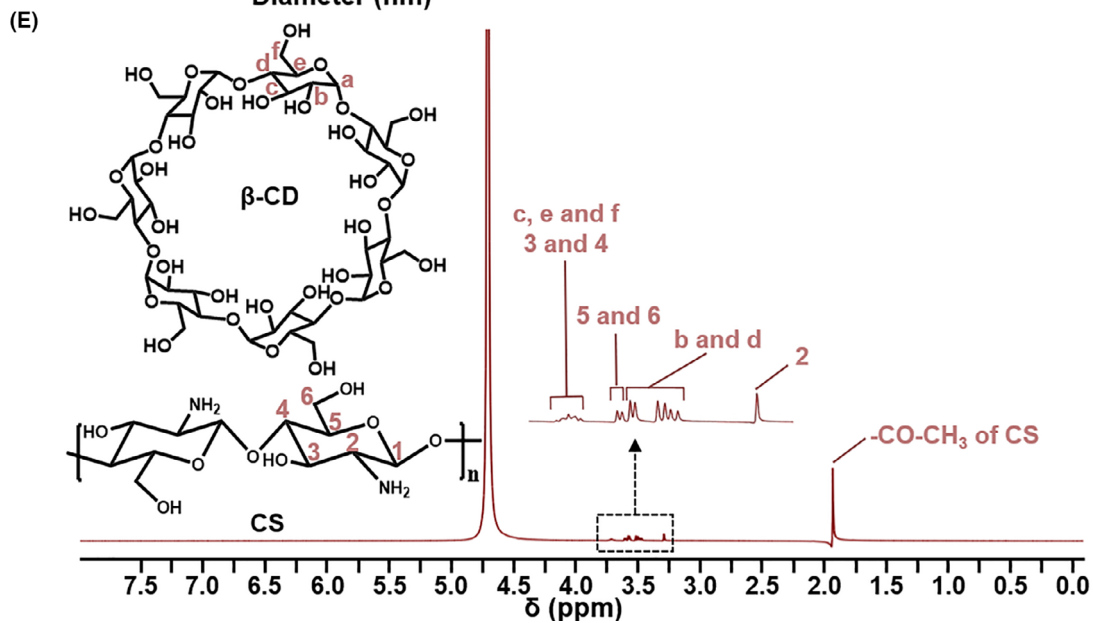
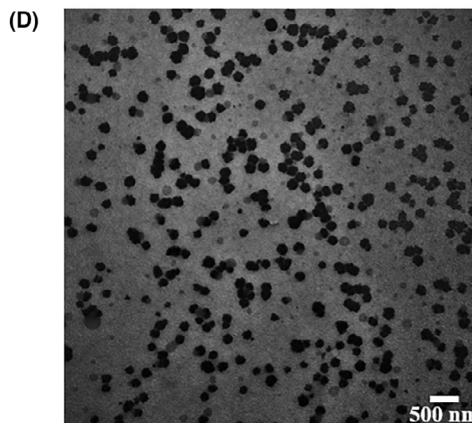
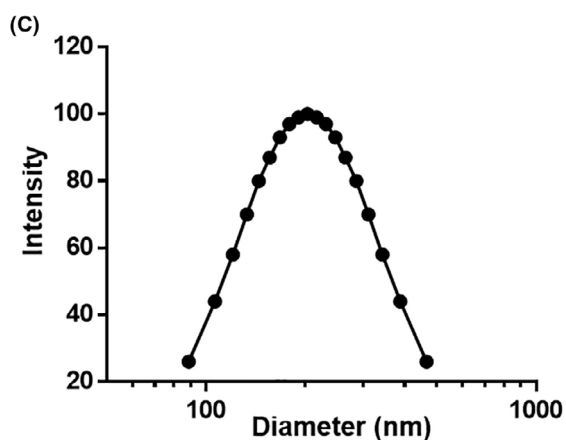
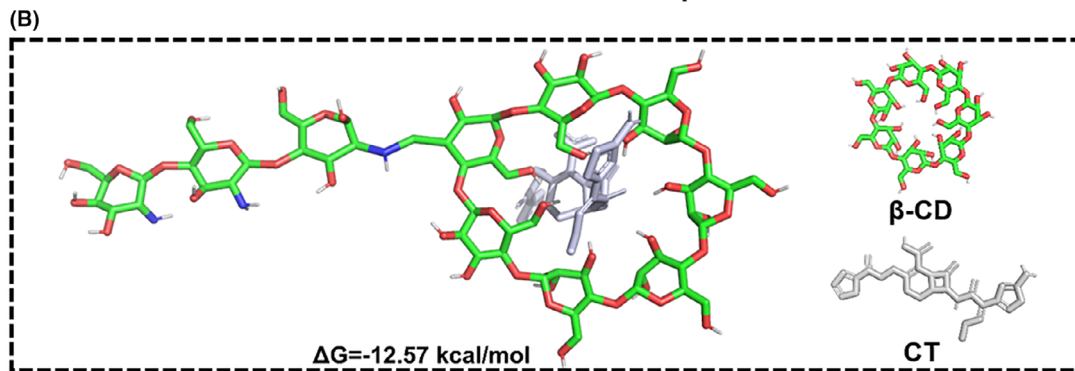
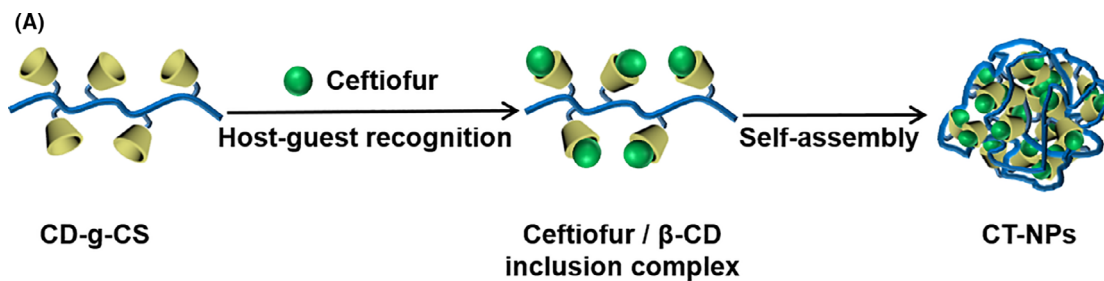


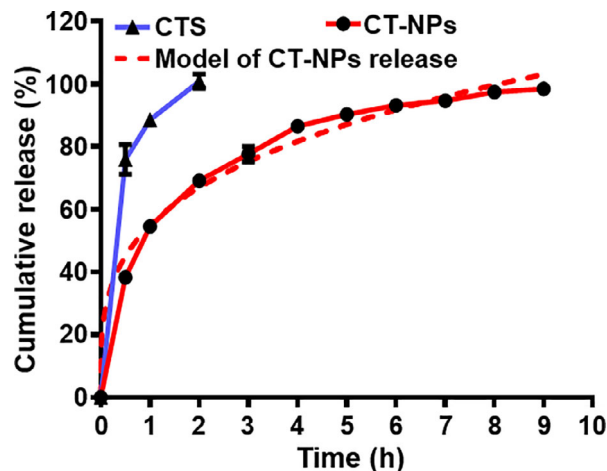
Fig. 1. Characterization of CT-NPs.

- A. Schematic illustration of the formation of CT-NPs.
 B. The structure of CT/CD-g-CS inclusion complexes, obtained via molecular docking.
 C. Diameter distribution of CT-NPs.
 D. TEM image of CT-NPs.
 E. ^1H NMR spectrum of CT-NPs in acetic acid-d₄.

further limiting its antibacterial efficacy (Zhang *et al.*, 2002).

The limitations of current antibiotic therapeutic strategies highlight the need to develop novel drug delivery systems to overcome the aforementioned problems. Among the drug delivery systems available today, polymer-based nanoparticles with chemical flexibility are the most suitable for enabling the development of unique treatments for bacterial infection. Chitosan (CS), a natural polycationic polysaccharide, has been widely used in the pharmaceutical and medical industries as a drug delivery carrier and antibacterial agent (Agnihotri *et al.*, 2004; Raafat and Sahl, 2010; Badawy *et al.*, 2014). Importantly, CS is positively charged at the infection site, which facilitates bacterial internalization (Carlson *et al.*, 2008; Ferreira *et al.*, 2010). In our previous work, a novel excipient, chitosan grafted with β -cyclodextrins (CD-g-CS), was synthesized. Ultimately, it proved to possess antibacterial activity and the ability to form inclusion complexes with drugs (Ding *et al.*, 2019). Thus, the use of CD-g-CS could be an alternative strategy for overcoming the drawbacks of CT, increasing antibacterial therapeutic efficacy.

As such, we demonstrated a novel drug delivery system using CD-g-CS as a nanocarrier for *S. xylo*-induced mastitis treatment. CTS was mixed with CD-g-CS in a weakly acidic solution, which allowed CTS to be protonated and changed into hydrophobic CT. Once this occurred, CT and β -cyclodextrin (β -CD) in CD-g-CS could form inclusion complexes via host-guest recognition. The resulting inclusion complex was amphiphilic and self-assembled into nanoparticles for CT encapsulation. We hypothesized that sustained release of CT could be achieved, which could allow for the maintenance of a sufficiently high drug concentration for increased effectiveness between injection intervals, and prevent biofilm formation. The CS in CD-g-CS also enhanced the bacterial uptake of nanoparticles and increased CT accumulation in bacteria. Therefore, ceftiofur-loaded CD-g-CS nanoparticles (CT-NPs) were expected to be more effective than CTS in treating *S. xylo* infections, both *in vitro* and *in vivo*. Compared to conventional CTS formulations, CT-NPs were more effective at killing planktonic *S. xylo*, effectively inhibiting biofilm formation and eliminating mature biofilms *in vitro*. They also enhanced the therapeutic efficacy of treatments for *S. xylo* infection when

**Fig. 2.** Cumulative release of CT from CD-g-CS nanoparticles *in vitro*.

administered at low dosages *in vivo*, which proved very useful for treating *S. xylo* in cases of cow mastitis.

Results and discussion

Characterization of CT-NPs

After the ultrasonic procedure, a clear light blue opalescence was observed in the mixed CTS and CD-g-CS acetic acid solution, indicating the formation of CT-NPs (Fig. S1). This finding revealed that CTS can be protonated and converted to CT in an aqueous acidic solution. We hypothesized that the resulting hydrophobic CT could be inserted into the cavity of β -CD in CD-g-CS via host-guest interaction, resulting in the formation of CT-NPs (Fig. 1A). To verify the above hypothesis, a molecular modelling method was used to confirm the interaction between β -CD in CD-g-CS and CT.

Typically, molecules with strong interactions exhibit more negative binding energy (Cui *et al.*, 2019). The binding energy of the CT-CD complexes was $-12.57 \text{ kcal}\cdot\text{mol}^{-1}$, indicating the existence of strong interactions (Chen *et al.*, 2017). According to the molecular modelling results, the possible conformation of CT-CD complexes with the lowest binding energy was constructed. As shown in Fig 1 B, CT was included in the cavity of β -CD in CD-g-CS at a molar ratio of 1:1, verifying the above hypothesis. The average diameter and zeta potential of CT-NPs was 230.3 nm and +24.75 mV, respectively, as determined by

laser particle size analysis (Fig. 1C). The morphologies and size of CT-NPs were visually observed using transmission electron microscope (TEM). All CT-NPs showed a clear spherical morphology, with an average diameter of approximately 230 nm (Fig. 1D); this is consistent with the particle size measured by laser particle size analysis.

Proton nuclear magnetic resonance (^1H NMR) was used to qualitatively determine the surface structure of CT-NPs. As shown in Fig. 1E, the proton signals of the CS and CT-CD complexes were simultaneously detected in the ^1H NMR spectrum of CT-NPs, which indicated the existence of CS and CT-CD complexes on the surface of the nanostructure.

In vitro drug release

CT-NPs release behaviours were investigated using the dialysis method, under the physiological condition of mastitis. The actual CT loading content (DL) and encapsulation efficiency (EE) were $2.56\% \pm 0.17\%$ and $71.5 \pm 2.18\%$, respectively. As shown in Fig. 2, owing to its high water solubility, CTS showed burst release behaviour and had approximately 100% release in 2 h. The cumulative release percentage of CT in CT-NPs only reached 68% in 2 h. This was followed by delayed release over a period of approximately 8 h. Burst release of a fraction of the dose (68%) after administration is favoured for the efficient killing of bacteria, reducing bacterial burden in the mastitis microenvironment (Fig. S2). Meanwhile, sustained release of the remaining dose will maintain sufficient drug concentration between injection intervals and prevent biofilm formation. To study the mechanism of sustained release behaviours, CT release profiles from CD-g-CS nanoparticles were analysed using the Korsmeyer–Peppas equation (1):

$$Q = kt^n \quad (1)$$

In this equation, Q is the drug fraction released at time t , k is a constant reflecting the characteristics of the CD-

g-CS nanoparticles, and n is the release exponent, which reflects the mechanism of drug release. Based on the parameter values obtained via non-linear regression analysis, the regression result was $Q = 54.86t^{0.2869}$ ($R^2 = 0.9874$), indicating a good fit for the Korsmeyer–Peppas equation. In addition, the value of n was less than 0.5, which demonstrated that CT release from CD-g-CS nanoparticles conformed to Fickian diffusion mechanisms. Thus, CT release was mainly attributed to the diffusion of the drug from the β -CD cavity and the nanoparticle matrix.

Stability study

The stability of the preparations was critical for their clinical application. Previous physicochemical property studies reported that CTS aqueous solutions can be stored for 12 h at 15–30°C, and for 7 days at 2–8°C (Brown *et al.*, 1996). The poor stability of CTS aqueous solutions seriously limits their application in clinical treatments. As shown in Fig. 3A, CTS concentration changes (C_1/C_0), and the relative drug loading content changes of CT-NPs (M_1/M_0) were used to demonstrate the stability of CTS and CT-NPs at room temperature (RT, 25°C) and 4°C, respectively. C_1/C_0 remained unchanged during storage at 4°C for 7 days, and gradually decreased at RT. The M_1/M_0 of CT-NPs remained unchanged during storage at 4°C for 15 days and at RT for 9 days (Fig. 3 B). These results demonstrate that CT-NPs could significantly improve the stability of CTS. The enhanced stability of CTS was partly attributed to the formation of CT and β -CD in CD-g-CS inclusion complexes, which could protect the drug from hydrolysis, oxidation and enzymolysis in the external environment (Aguiar *et al.*, 2014; Guendouzi *et al.*, 2020). Additionally, the repulsive force between the positively charged surfaces could prevent the agglomeration or precipitation of CT-NPs, thereby increasing the stability of the nanoparticles in aqueous solutions.

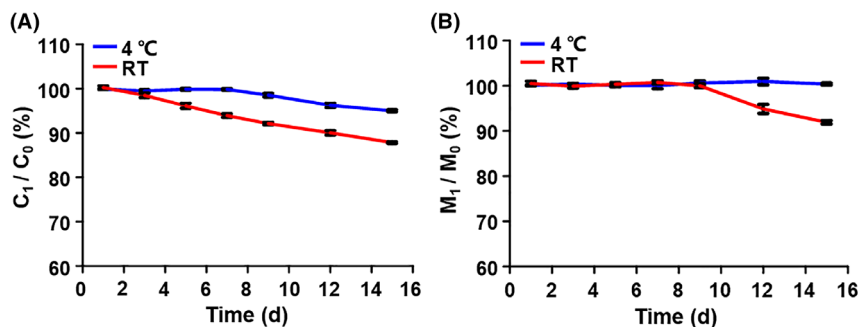


Fig. 3. Stability of CTS and CT-NPs at 4°C and RT (25°C), respectively.
A. Relative concentration changes in CTS aqueous solution after storage for various periods of time.
B. Relative drug loading content changes in CT-NPs after storage for various periods of time.

Internalization of CT-NPs by *S. xylosus*

Previous studies have demonstrated that CS can effectively enhance drug absorption by increasing membrane permeability through amino groups (Huang *et al.*, 2004; Schipper *et al.*, 1996; Je and Kim, 2006; Chen *et al.*, 2017). Therefore, internalization of CT-NPs was

qualitatively examined via confocal laser scanning microscopy (CLSM). Coumarin-6 (CM-6) was utilized as a model fluorescence drug to construct nanoparticles with CD-g-CS. *S. xylosus* specimens incubated with CM-6 loaded CD-g-CS nanoparticles (CM-6-NPs) for 2 h showed distinctly stronger CM-6 fluorescence than those treated with free CM-6 (Fig. 4A). To learn more about

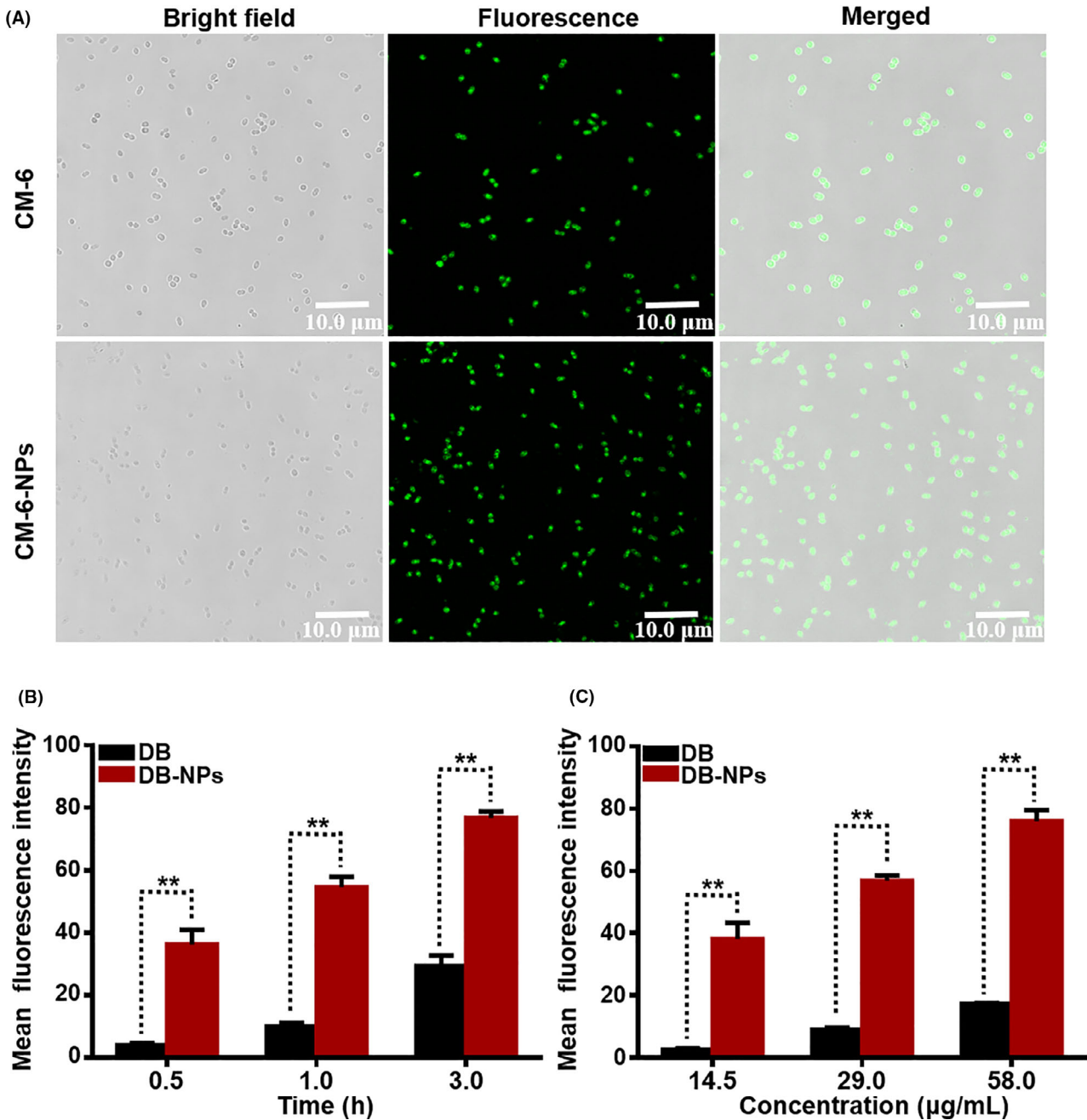


Fig. 4. Internalization ability of CT-NPs by *S. xylosus*.

A. CLSM images of *S. xylosus* after incubation with CM-6 and CM-6-NPs for 2 h.

B. Mean fluorescence intensity in *S. xylosus* after incubation with DB and DB-NPs with equivalent DB dosage ($29 \mu\text{g ml}^{-1}$) for different intervals.

C. Mean fluorescence intensity in *S. xylosus* after incubation with different concentrations of DB and DB-NPs for 1.0 h. ** $P < 0.01$.

the effect of time and drug concentration on bacterial uptake, bacterial accumulation of doxorubicin (DB) and DB-loaded CD-g-CS nanoparticles (DB-NPs) was quantitatively assessed using flow cytometry. As shown in Fig. 4B, *S. xylosus* treated with DB-NPs displayed stronger fluorescence flow cytometry intensity than *S. xylosus* treated with DB after incubation at multiple time-points. Especially, after 0.5 h of incubation, *S. xylosus* treated with DB-NPs showed 8.6-fold stronger fluorescence intensity than *S. xylosus* treated with free DB. The effect of concentration on nanoparticle uptake was also further investigated. As shown in Fig. 4C, *S. xylosus* specimens treated with DB-NPs had distinctly stronger fluorescence intensities than those treated with free DB at all tested concentrations. Meanwhile, the counting level of the DB-NPs in *S. xylosus* increased as incubation concentration increased. These results demonstrate that DB-NPs, with CD-g-CS as a nanocarrier, markedly enhanced bacterial internalization.

The antibacterial effect of CT-NPs on planktonic S. xylosus

The minimum inhibitory concentration (MIC) represents the lowest concentration of antimicrobial agents required to inhibit bacterial growth (Al-Yousef, *et al.*, 2017). To quantify their antibacterial effects, the MIC values of both CT-NPs and CTS were determined. The MIC values of CTS and CT-NPs against *S. xylosus* were 0.50 and 0.25 $\mu\text{g ml}^{-1}$, respectively. Compared with free CTS, the superior antibacterial activity of CT-NPs was contributed to proposed mechanisms. On one hand, CT-NPs with positively charged surfaces can interact with bacterial cell membranes, increase their permeability, and promote bacterial uptake of CT. On the other hand, the CS in the CD-g-CS of CT-NPs possesses intrinsic antibacterial qualities, which could cause leakage of bacterial components and achieve synergistic antibacterial effects with CT (Gonil *et al.*, 2011; Chen *et al.*, 2017; Ding *et al.*, 2019).

Inhibition biofilm formation of S. xylosus

Under physiological conditions, *S. xylosus* readily produces EPS and forms biofilms. Therefore, inhibition of *S. xylosus* biofilm formation is very important for treating mastitis in cows. As shown in Fig. 5A, both CTS and CT-NPs inhibited biofilm formation in a concentration-dependent manner when *S. xylosus* was incubated with CTS and CT-NPs under biofilm formation conditions for 24 h. CT-NPs displayed more obvious inhibitory effects than CTS at all tested concentrations, as expected. Such finding indicated the positive role that nanoparticles can play in the inhibition of *S. xylosus* biofilm formation. Even at the low CT concentration of 0.03125 $\mu\text{g ml}^{-1}$, CT-NPs

displayed more significant inhibitory effects than CTS (39.9% vs. 17.6%, respectively). In particular, CT-NPs resulted in a biofilm reduction of 47.6% at a concentration of 0.125 $\mu\text{g ml}^{-1}$, exhibiting remarkable potential for inhibiting *S. xylosus* biofilm formation at low dosages.

Furthermore, the morphology of *S. xylosus*, when treated with CT-NPs, was examined using scanning electron microscopy (SEM). As shown in Fig. 5B and Fig. S3, thick and well-formed biofilms were observed at 24 h, indicating the development of mature biofilms in the control group. Conversely, biofilm formation was inhibited upon exposure to CT-NPs of 0.0625 $\mu\text{g ml}^{-1}$, and existing biofilms became thin and disintegrated. *S. xylosus* treated with 0.125 $\mu\text{g ml}^{-1}$ CT-NPs showed only slight bacterial aggregation. However, well-formed biofilms was still observed in the group treated with 0.125 $\mu\text{g ml}^{-1}$ CTS. It was clear that CT-NPs had better inhibition efficacy than CTS, which was consistent with the results of the crystal violet staining assay. The enhanced ability of CT-NPs to inhibit biofilm formation might be attributed to their ability to reduce the secretion of exopolysaccharides, which are key substances in bacterial biofilm formation (Xie *et al.*, 2017).

Elimination of S. xylosus biofilm

It is well known that biofilms can hinder the penetration of antimicrobial agents and make bacteria in biofilm insensitive to most antibiotics, resulting in both the recurrence and incurability of *S. xylosus* infections (Kouidhi *et al.*, 2015; Xu *et al.*, 2017). However, nanocarriers with positively charged surfaces readily interact with negatively charged EPS, improving the ability of drugs to penetrate biofilms (Ferreira *et al.*, 2010). Therefore, the ability of CT-NPs to eradicate mature *S. xylosus* biofilms was evaluated. Considering the reduced sensitivity of antibacterial agents when employed against biofilm bacteria, only CT-NPs with concentrations of 1 and 2 $\mu\text{g ml}^{-1}$ were involved in the anti-mature biofilm test. Biofilm biomass decreased in a dose-dependent manner when treated with CTS and CT-NPs (Fig. 6). As expected, the eradication effect of CT-NPs significantly improved compared to that of CTS. CT-NPs reduced the biofilm mass to 69% (1 $\mu\text{g ml}^{-1}$) and 56% (2 $\mu\text{g ml}^{-1}$) at 12 h, respectively. However, CTS at equal concentrations only reduced the biofilm mass to 83% (1 $\mu\text{g ml}^{-1}$) and 74% (2 $\mu\text{g ml}^{-1}$). Compared with planktonic bacteria (MIC of 0.25 $\mu\text{g ml}^{-1}$), the antibacterial effect of CT-NPs was reduced in the presence of mature biofilm.

Antibacterial activity of CT-NPs in mouse mastitis model

The *in vivo* antibacterial effect of CT-NPs was determined in a mouse mastitis model. In clinical therapy,

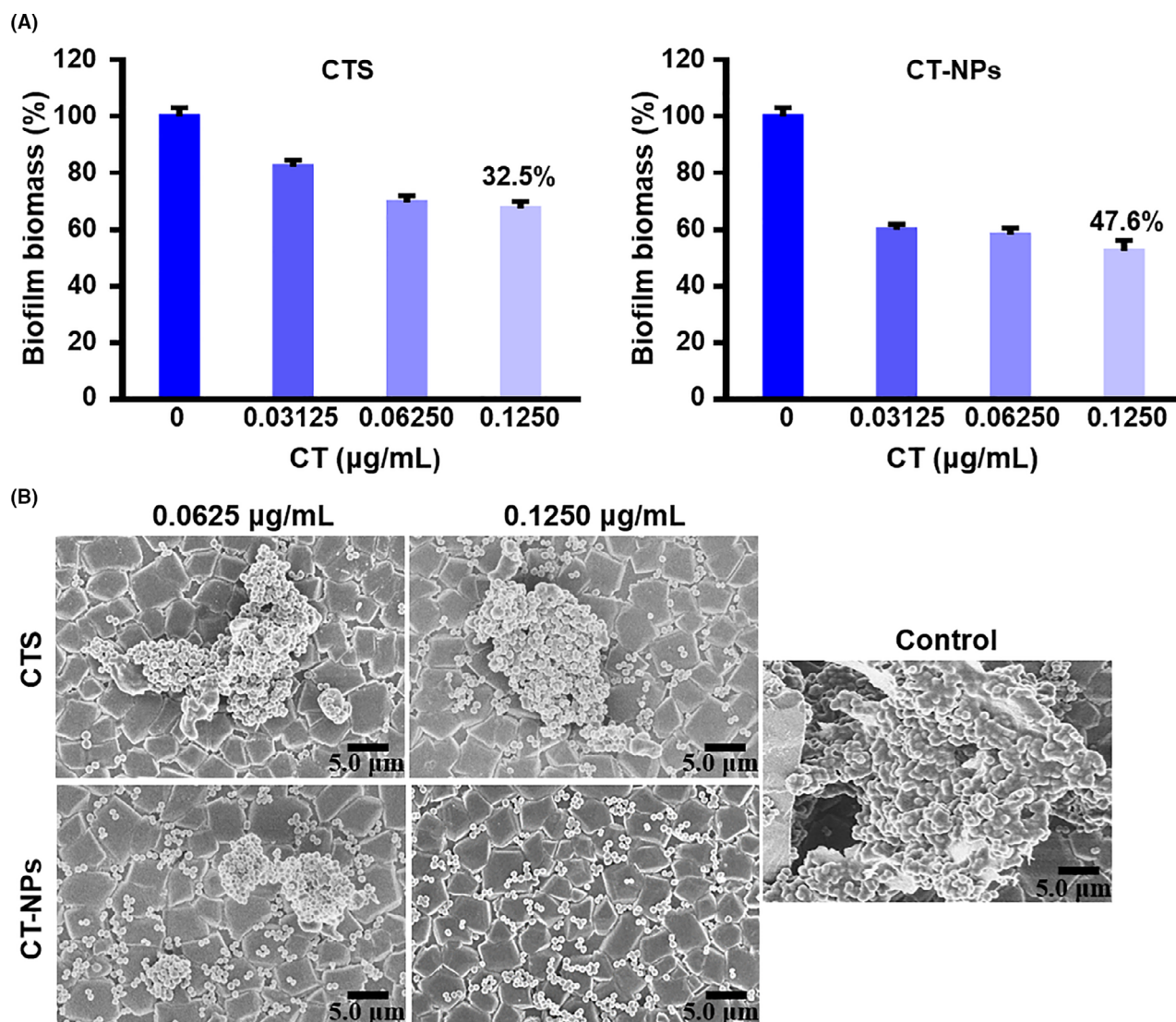


Fig. 5. The inhibitory effects of CT-NPs on *S. xylosum* biofilm formation *in vitro*.

A. Inhibition of *S. xylosum* biofilm biomass by CTS and CT-NPs at different concentrations.

B. SEM images of *S. xylosum* biofilm biomass after incubation with CTS and CT-NPs with equivalent CTS concentrations (0.0625 and 0.1250 $\mu\text{g ml}^{-1}$, respectively) for 24 h.

intramammary infusion is a normal procedure for treating cow mastitis. Therefore, CT-NPs were directly injected into pathological mammary tissue to address clinical requirements after *S. xylosum*-induced mastitis was identified (Fig. 7A). After treatment for 24 h, mice were sacrificed and their mammary glands were macroscopically observed and histologically analysed. As shown in Fig. 7B, the mammary glands of mice treated with CT-NPs had almost returned to normal, whereas the mammary glands of mice in the CTS group were slightly red. Furthermore, to objectively evaluate the inhibitory effects of CTS and CT-NPs, micrographs of haematoxylin and eosin (H&E)-stained mammary gland sections were collected. As expected, no inflammatory changes were

observed in the CT-NPs group. Although CTS could also alleviate *S. xylosum*-induced inflammatory responses in infected mice, we observed the presence of exudate in acinar tissues, as well as obvious acinar wall hyperplasia (green arrow).

Tumour necrosis factor α (TNF- α) and interleukin-6 (IL-6) are key markers of inflammation (Sakemi *et al.*, 2011; Oskarsson *et al.*, 2017), and their levels in the mammary glands significantly decreased, returning to normal levels, after CT-NPs treatment (Fig. 7C and D). The colony count results further confirmed the therapeutic effect of CT-NPs. *S. xylosum* counts in the mammary glands of the control group were 9.6×10^6 CFUs g^{-1} tissue, while a significant decrease in *S. xylosum* counts

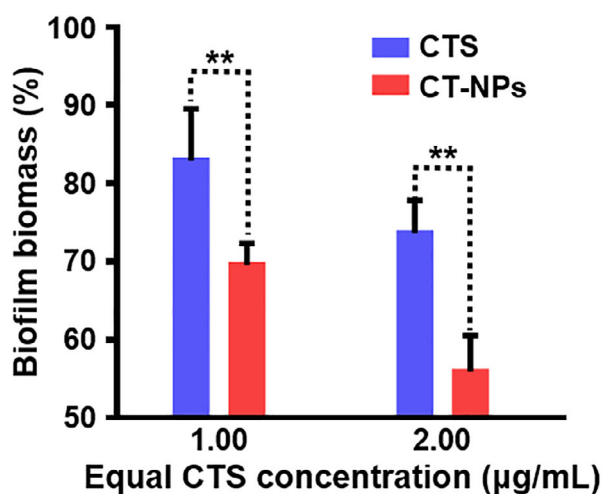


Fig. 6. Elimination of *S. xylosois* biofilm biomass by CTS and CT-NPs at different concentrations. ** $P < 0.01$.

was observed in drug-treated mammary glands. More importantly, the average *S. xylosois* count in the mammary glands of infected mice treated with CT-NPs was 1.1×10^5 CFUs g^{-1} tissue. This was far less than the average *S. xylosois* count of 1.5×10^6 CFUs g^{-1} tissue detected in mammary glands treated with CTS (Fig. 7E). These results demonstrate that CT-NPs possess enhanced anti-inflammatory effects in cases of *S. xylosois*-induced mastitis, regulating the expression of $TNF-\alpha$ and $IL-6$ and reversing damage to mammary glands and mammary epithelial cells. Altogether, the findings clearly demonstrate the enhanced antibacterial efficacy of CT-NPs for treating mammary tissue infected with *S. xylosois*.

Conclusions

In summary, we successfully fabricated a novel ceftiofur delivery platform for the efficient treatment of *S. xylosois* infections. CT-NPs with positive surface charges could improve bacterial internalization, and in turn enhance the killing efficacy of antibiotic treatments against *S. xylosois*. Meanwhile, CT-NPs prolonged ceftiofur release, effectively inhibiting biofilm formation and eliminating *S. xylosois* biofilms *in vitro*. After administrated in a *S. xylosois* mastitis model, the CT-NPs exhibited enhanced therapeutic efficacy compared to conventional ceftiofur sodium formulations. This work suggests the promising prospect of using ceftiofur for enhanced *S. xylosois* infection therapy.

Experimental procedures

Materials, media, and organisms

Staphylococcus xylosois ATCC 700404 was purchased from the American Type Culture Collection. Chitosan

(MW = 150 kDa, the deacetylation degree was above 90%) was obtained from Beijing Biotopped Science & Technology Co. Ltd (Beijing, China). β -Cyclodextrin was purchased from Sinopharm Chemical Reagent Co. Ltd (Shanghai, China). P-toluenesulphonyl chloride was purchased from Shanghai Macklin Biochemical Co. Ltd (Shanghai, China). Doxorubicin and ceftiofur sodium were purchased from Shanghai Yuan Ye Biochemical Co. Ltd (Shanghai, China). Acetic acid, dimethyl sulfoxide (DMSO) and acetone were purchased from Tianjin Kernel Analytical Reagent Co. Ltd (Tianjin, China). Trypticase Soy broth (TSB) was purchased from Summus Ltd (Harbin, China). Kunming mice were obtained from the Second Affiliated Hospital of the Harbin Medical University. ELISA kits for $IL-6$ and $TNF-\alpha$ were purchased from Quanzhou Konuodi Biotechnology Co., Ltd (Quanzhou, China).

Preparation of CD-g-CS

CD-g-CS was synthesized using previously reported methods in our laboratory (Fig. S4) (Ding *et al.*, 2019). β -CD (2.5 g) was suspended in DMSO (6.5 ml) and 3.75 g of p-toluenesulphonyl chloride in DMSO (6 ml) was added dropwise. The solution was stirred at 45°C for 24 h, and then acetone (30 ml) was added dropwise. The solution crystallized immediately, and a white precipitate was observed. The white precipitate was filtered and rinsed with precooled acetone. This procedure was repeated three times to obtain mono-6-deoxy-6-(p-toluenesulphonyl)- β -cyclodextrin (6-OTs- β -CD).

CS (0.25 g) was dissolved in 1% (v/v) acetic acid. The prepared 6-OTs- β -CD was added to the CS/acetic acid solution, and the reaction mixture was stirred at 45°C for 48 h. Thereafter, the solution was dialysed against deionized water for 7 days to remove DMSO, acetone, unreacted β -CD, and p-toluenesulphonyl chloride, before being freeze-dried for further analysis. The structures of the products were confirmed via 1H NMR spectroscopy (Fig. S5).

Preparation of drug loaded CD-g-CS nanoparticles

CD-g-CS solution (5 mg ml^{-1}) was prepared by dissolving CD-g-CS in acetic acid (2%, v/v). Thereafter, the pH value of the solution was adjusted to 4.5 with NaOH (8 M). Subsequently, CTS (1 mg) was dissolved in methanol (1 ml) and added to the CD-g-CS solution. After removing the methanol using rotary evaporation, the solution was magnetically stirred at 25°C for 2 h and then ultra-sounded for another 10 min. Finally, the solution was centrifuged to obtain the CT-NPs. Meanwhile, DB-NPs and CM-6-NPs were prepared using a similar process.

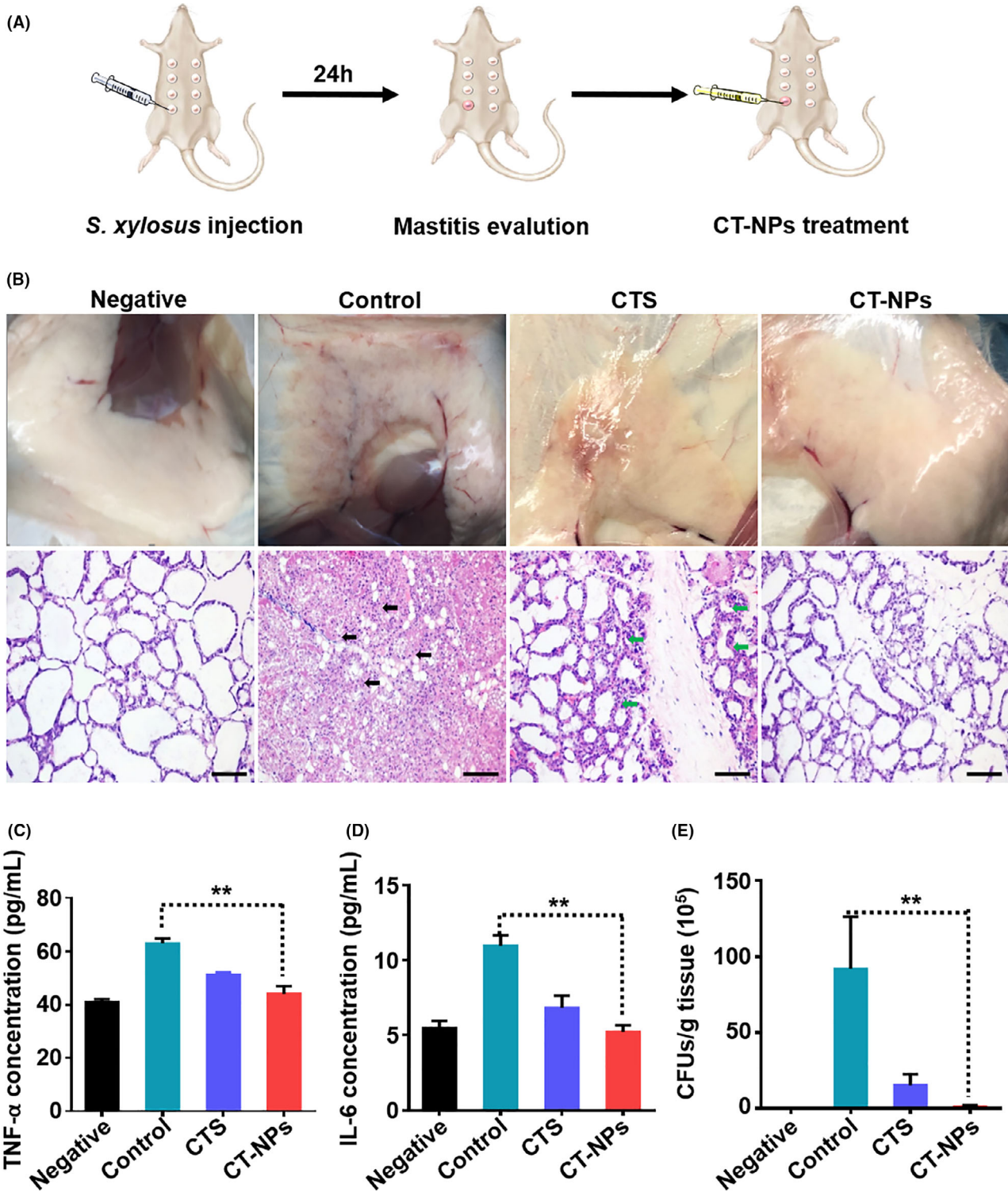


Fig. 7. Anti-infection efficacy of CT-NPs in a *S. xylo*sus mastitis model *in vivo*.

A. Schematic illustration of the establishment of *S. xylo*sus-induced mastitis, and efficacy evaluation.

B. Photographs and histological assessment of mammary glands with H&E staining. Alteration of levels of TNF- α (C), IL-6 (D), and bacterial quantity (E) in the mammary glands of different experimental groups. ** $P < 0.01$.

Molecular modelling

The mechanism of CT-NPs formation was investigated via molecular modelling using CDOCKER in Discovery Studio 3.0. The molecular structures of CT and β -CD were obtained from PubChem and the Cambridge Structural Database (ref. code BCDEX03). The coordinates of the grid ball were X: 3.305, Y: 0.4165, and Z: 0.0976. The radius of the ball was 15 Å, and the grid ball itself was large enough to both include the cavity portion and cover the entire surface of β -CD. After 100 docking runs, as counted by the scoring function, the final optimal docking result was selected for analysis. A semiempirical auto-dock free energy force field was used to estimate the interaction free energy and the conformer with the lowest binding energy in relation to the ligand was used for further analysis.

Characterization of CT-NPs

The prepared CT-NPs solution was diluted with phosphate-buffered saline (PBS, pH = 7.4) to a final concentration of 323.7 $\mu\text{g ml}^{-1}$. The average size and zeta potential of the diluted CT-NPs were measured using laser particle size analysis. For TEM measurement, the concentration of CT-NPs was adjusted to 1.3 mg ml^{-1} . Finally, the solution was stained with 1.5% (w/v) phosphotungstic acid and dropped onto a copper grid for morphological observation.

To evaluate the CT DL and EE, free CT was separated from its nanoparticle suspensions via centrifugation at 10 000 rpm for 30 min. The amount of CT remaining in the supernatant was measured using a UV spectrophotometer, with each sample measured three times. The EE and DL were calculated using the following Equations (2) and (3):

$$\text{EE}(\%) = \frac{(\text{total weight of CT} - \text{weight of free CT})}{\text{total weight of CT}} \quad (2)$$

$$\text{DL}(\%) = \frac{(\text{total weight of CT} - \text{weight of free CT})}{\text{weight of CT} - \text{NPs}} \quad (3)$$

In vitro release studies

A CT-NPs solution (5 ml) was briefly sealed into a dialysis membrane (MWCO = 14 000 Da), which was immersed in 45 ml of release medium (PBS, pH = 6.5). The experiment was conducted in a shaking incubator at a shaking speed of 100 rpm, with a constant temperature of 37°C. At predefined time intervals, 5 ml of the outside solution was withdrawn and replaced with fresh release medium (5 ml). The concentration of the

released drug was determined using UV. The release profile of free CTS was studied as a control.

Stability study

CT-NPs solution and CTS aqueous solution with the same CTS content were placed at 4°C and RT, respectively. At predefined time intervals, the CT DL of the CT-NPs and the concentration change of the CTS aqueous solution were measured using a UV spectrophotometer, as described above.

Determination of MIC

MIC, which is defined as the lowest concentration of an antimicrobial agent that prevents the growth of bacteria, was determined using a microtiter broth dilution method. In brief, *S. xylosus* was harvested, and adjusted to a density of 1×10^5 CFU ml^{-1} . Thereafter, 180 μl of the bacterial suspension was inoculated into each well of a 96-well plate. Subsequently, 20 μl CTS or CT-NPs solutions with equal CT concentrations (0.625–80 $\mu\text{g ml}^{-1}$) were added. The treated *S. xylosus* specimens were then incubated under aerobic conditions at 37°C with shaking and were used for turbidity observations after 24 h.

Bacterial uptake

S. xylosus was incubated in 6-well plates with CM-6 and CM-6-NPs (at a final CM-6 concentration of 40 $\mu\text{g ml}^{-1}$) at 37°C for 2 h. Subsequently, the *S. xylosus* solutions were centrifuged, washed three times with PBS, and resuspended in 500 μl PBS. Fluorescence images were obtained using CLSM.

For flow cytometry analysis, *S. xylosus* was treated with DB and DB-NPs at different DB concentrations (14.5, 29 and 58 $\mu\text{g ml}^{-1}$), and incubated at 37°C for 1 h. At the same time, DB and DB-NPs with equal DB concentrations (29 $\mu\text{g ml}^{-1}$) were co-incubated with *S. xylosus* for 0.5, 1, and 3 h. Thereafter, *S. xylosus* was centrifuged. The *S. xylosus* specimens obtained through centrifugation were treated with three cycles of PBS washing and centrifugation, before finally being resuspended in 500 μl PBS for flow cytometry analysis.

Inhibition of biofilm formation

The biofilm inhibition experiment was performed by seeding 100 μl of *S. xylosus* suspension and 100 μl of CTS or CT-NPs into each well on a 96-well microplate. The final concentrations of CTS and CT-NPs with equal CTS were 0.03125, 0.06250 and 0.1250 $\mu\text{g ml}^{-1}$, respectively. After incubation at 37°C for 24 h without shaking,

the supernatants were removed. The wells were rinsed with 50 mM PBS (pH = 7.2), fixed with 200 μ l methanol for 30 min, and stained with 200 μ l 1% crystal violet (*w/v*) for 30 min. They were then rinsed three times with PBS and dried at 37°C for 2 h. Thereafter, 200 μ l of 33% acetic acid (*v/v*) was added and the microplate was shaken for 10 min. The contents of all wells were measured using a Tecan GENios Plus Microplate Reader (Tecan, Austria) set to 595 nm. A *S. xylosus* suspension with bacteria alone was used as control.

The effect that CT-NPs have on biofilm formation was further examined using SEM. Briefly, overnight cultures of *S. xylosus* were diluted in TSB. Thereafter, the culture medium was supplemented with CT-NPs and CTS at final concentrations of 0.0625 and 0.1250 μ g ml⁻¹ in the medium, respectively, and 2 ml of the resulting solution was added to the wells of a 6-well microplate. Each well contained a 10 \times 10 mm sterilized, rough organic membrane at the bottom. After incubation, without shaking for 24 h at 37°C, the organic membranes (with biofilms grown on them) were removed from the wells. Thereafter, medium and planktonic bacteria on the membranes were removed by washing the membranes with sterile PBS. The biofilms were incubated in 2.5% (*w/v*) glutaraldehyde for 1.5 h at 4°C, and washed three times with 0.1 M cacodylate buffer (pH = 7.0) for 20 min each time. The biofilms were then dehydrated using a graded series of ethanol (50%, 70%, 95% and 100%), ethanol and tertiary butyl alcohol mixed solution (1:1, *v/v*) and tertiary butyl alcohol. The dehydrated samples were subjected to critical point drying and gold sputtering. Finally, the biofilms were observed using SEM.

Elimination of biofilm

Biofilms were formed by adding 200 μ l of TSB solution containing *S. xylosus* into 96-well microplates and incubating them at 37°C for 24 h, without shaking. CT-NPs and CTS were then added to the wells at final concentrations of 1 and 2 μ g ml⁻¹, respectively. Biofilms incubated with PBS were used as controls. After cultivation at 37°C for 12 h, a crystal violet staining assay was used to detect biofilm mass. Each test was repeated three times.

Establishment of a mouse mastitis model

Kunming mice that gave birth on the 7th day were obtained from the experimental animal centre of the Second Affiliated Hospital of Harbin Medical University. All animal experiments involved in this experiment were approved by the experimental animal research ethics committee of Northeast Agricultural University (SRM-11). And all animal procedures complied with the ARRIVE

guidelines, and were carried out in accordance with the National Institute of Health Guide for the Care and Use of Laboratory Animals (NIH Publications No. 8023, revised 1978), as well as the CONSORT (Consolidated Standards of Reporting Trials) statement (Kilkenny *et al.*, 2012; Moher *et al.*, 2012). The animals were kept under standard conditions with free access to water and food.

Kunming mice were randomly divided into four groups (*n* = 5). Mice with mastitis used in this experiment had their mastitis induced via the injection of 100 μ l (1×10^9 CFU ml⁻¹) of *S. xylosus* suspension into the canal glands at the 4th breast on both sides. This occurred over the course of 24 h, and after anaesthesia. Healthy mice were used as negative controls.

In vivo effect of CT-NPs on mastitis

After being injected with *S. xylosus* suspensions (100 μ l, 1×10^9 CFU ml⁻¹) for 24 h, the mouse mastitis model was successfully established. CTS and CT-NPs were administered by injecting equivalent CTS dosages (100 μ l, 0.25 μ g ml⁻¹) into the mastitis-afflicted 4th breasts over the course of another 24 h. Mice with mastitis in the control group were not subjected to any treatment.

Pathological changes in all mice were monitored. At the end of the experimental period, which included the establishment and treatment of the mastitis models, mice were sacrificed. Mammary gland tissues were collected, fixed in 4% paraformaldehyde solution, and then embedded in paraffin. The paraffin-embedded tissues were each cut into 2 sections, and then stained with H&E. The stained slices were assessed using a microscope. Furthermore, additional mammary gland tissues were homogenized in normal saline. Thereafter, they were partially diluted, and inoculated onto TSB agar plates to assess their bacterial load. Inflammatory cytokine (IL-6 and TNF- α) levels in the supernatant were measured using ELISA kits.

Statistical analysis

Statistical analyses were conducted using Microcal Origin v. 7.5 (OriginLab Corp, Northampton, MA, USA). The data obtained were analysed for significance using one-way analysis of variance (ANOVA). Values are reported as mean \pm standard deviation, and statistical means were compared using *t*-tests, with *P* < 0.05 considered statistically significant.

Acknowledgements

This work was supported by the National Natural Science Foundation of China (No. 31802228), the

Chinese Postdoctoral Science Foundation (2019M661246), the Guangxi University of Chinese medicine foundation for the introduction of doctoral research (2019BS006) and the earmarked fund for China Agriculture Research System-35.

Funding Information

This work was supported by the National Natural Science Foundation of China (No.31802228), the Chinese Postdoctoral Science Foundation (2019M661246), the Guangxi University of Chinese medicine foundation for the introduction of doctoral research (2019BS006) and the earmarked fund for China Agriculture Research System-35.

Conflict of interest

The authors declare no conflict of interest.

References

- Agnihotri, S.A., Mallikarjuna, N.N., and Aminabhavi, T.M. (2004) Recent advances on chitosan-based micro- and nanoparticles in drug delivery. *J Control Release* **99**: 5–28.
- Aguiar, U.N., de Lima, S.G., Rocha, M.S., de Freitas, R.M., Oliveira, T.M., Silva, R.M., *et al.* (2014) Preparation and characterization of the inclusion complex essential oil of croton zehntneri with beta-cyclodextrin. *Quim Nova* **37**: 50–55.
- Akhaddar, A., Elouennass, M., Naama, O., and Boucetta, M. (2010) *Staphylococcus xylosus* isolated from an otogenic brain abscess in an adolescent. *Surg Infect* **11**: 559–561.
- Al-Yousef, H.M., Ahmed, A.F., Al-Shabib, N.A., Laeeq, S., Khan, R.A., Rehman, M.T., *et al.* (2017) Onion peel ethylacetate fraction and its derived constituent quercetin 4'-O-beta-D glucopyranoside attenuates quorum sensing regulated virulence and biofilm formation. *Front Microbiol* **8**: 1675.
- Badawy, M.E.I., Rabea, E.I., and Taktak, N.E.M. (2014) Antimicrobial and inhibitory enzyme activity of N-(benzyl) and quaternary N-(benzyl) chitosan derivatives on plant pathogens. *Carbohydr Polym* **111**: 670–682.
- Brown, S., Chester, S.T., and Robb, E.J. (1996) Effects of age on the pharmacokinetics of single dose ceftiofur sodium administered intramuscularly or intravenously to cattle. *J Vet Pharmacol Ther* **19**: 32–38.
- Carlson, R.P., Taffs, R., Davison, W.M., and Stewart, P.S. (2008) Anti-biofilm properties of chitosan-coated surfaces. *J Biomater Sci-Polym Ed* **19**: 1035–1046.
- Chen, P., Song, H., Yao, S., Tu, X., Su, M., and Zhou, L. (2017) Magnetic targeted nanoparticles based on beta-cyclodextrin and chitosan for hydrophobic drug delivery and a study of their mechanism. *Rsc Adv* **7**: 29025–29034.
- Cui, W.-Q., Qu, Q.-W., Wang, J.-P., Bai, J.-W., Bello-Onaghise, G., Li, Y.-A., *et al.* (2019) Discovery of potential anti-infective therapy targeting glutamine synthetase in *Staphylococcus xylosus*. *Front Chem* **7**: 381.
- Ding, W.Y., Zheng, S.D., Qin, Y., Yu, F., Bai, J.W., Cui, W.Q., *et al.* (2019) Chitosan Grafted with beta-cyclodextrin: synthesis, characterization, antimicrobial activity, and role as absorbent and solubilizer. *Front Chem* **6**: 657.
- Ferreira, C., Pereira, A. M., Melo, L. F., and Simões, M. (2010) Advances in industrial biofilm control with micro-nanotechnology. *Curr Res, Technol and Educ Top in Appl Microb and Microb Biotechnol* **30**: 327–356.
- Flemming, H.C., Wingender, J., Szewzyk, U., Steinberg, P., Rice, S.A., and Kjelleberg, S. (2016) Biofilms: an emergent form of bacterial life. *Nat Rev Microbiol* **14**: 563–575.
- Flores-Orozco, D., Patidar, R., Levin, D.B., Sparling, R., Kumar, A., and Cicek, N. (2020) Effect of ceftiofur on mesophilic anaerobic digestion of dairy manure and the reduction of the cephalosporin-resistance gene *cmx-2*. *Bioresour Technol* **301**: 122729.
- Gonil, P., Sajomsang, W., Ruktanonchai, U.R., Pimpha, N., Sramala, I., Nuchuchua, O., *et al.* (2011) Novel quaternized chitosan containing beta-cyclodextrin moiety synthesis, characterization and antimicrobial activity. *Carbohydr Polym* **83**: 905–913.
- Guendouzi, O., Guendouzi, A., Ouici, H.B., Brahim, H., Boumediene, M., and Elkeurti, M. (2020) A quantum chemical study of encapsulation and stabilization of gallic acid in beta-cyclodextrin as a drug delivery system. *Can J Chem* **98**: 204–214.
- Helbling, I.M., Busatto, C.A., Karp, F., Islan, G.A., Estenez, D.A., and Luna, J.A. (2020) An analysis of the microencapsulation of ceftiofur in chitosan particles using the spray drying technology. *Carbohydr Polym* **234**: 115922.
- Huang, M., Khor, E., and Lim, L.Y. (2004) Uptake and Cytotoxicity Of Chitosan Molecules And Nanoparticles: Effects Of Molecular Weight And Degree Of Deacetylation. *Pharm Res* **21**: 344–353.
- Je, J.Y., and Kim, S.K. (2006) Chitosan derivatives killed bacteria by disrupting the outer and inner membrane. *J Agr Food Chem* **54**: 6629–6633.
- Kilkenny, C., Browne, W.J., Cuthill, I.C., Emerson, M., and Altman, D.G. (2012) Improving bioscience research reporting: the ARRIVE guidelines for reporting animal research. *Osteoarthritis Cartilage* **20**: 256–260.
- Kouidhi, B., Al Qurashi, Y.M.A., and Chaieb, K. (2015) Drug resistance of bacterial dental biofilm and the potential use of natural compounds as alternative for prevention and treatment. *Microb Pathogenesis* **80**: 39–49.
- Locatelli, C., Barberio, A., Bonamico, S., Casula, A., Moroni, P., and Bronzo, V. (2019) Identification of multidrug-resistant *Escherichia coli* from bovine clinical mastitis using a ceftiofur-supplemented medium. *Foodborne Pathog Dis* **16**: 590–596.
- Makovcova, J., Babak, V., Kulich, P., Masek, J., and Cincarova, L. (2017) Dynamics of mono- and dual-species biofilm formation and interactions between *Staphylococcus aureus* and Gram-negative bacteria. *Microb Biotechnol* **10**: 819–832.
- Moher, D., Hopewell, S., Schulz, K.F., Montori, V., Gøtzsche, P.C., Devereaux, P.J., *et al.* (2012) CONSORT 2010 explanation and elaboration: Updated guidelines for reporting parallel group randomised trials. *Int J Surg* **10**: 28–55.

- Oskarsson, A., Yagdiran, Y., Nazemi, S., Talkvist, J., and Knight, C.H. (2017) Short communication: Staphylococcus aureus infection modulates expression of drug transporters and inflammatory biomarkers in mouse mammary gland. *J Dairy Sci* **100**: 2375–2380.
- Osman, K.M., Abd El-Razik, K.A., Marie, H.S.H., and Arafa, A. (2016) Coagulase-negative staphylococci collected from bovine milk: species and antimicrobial gene diversity. *J Food Safety* **36**: 89–99.
- Parsek, M.R., and Singh, P.K. (2003) Bacterial biofilms: an emerging link to disease pathogenesis. *Annu Rev Microbiol* **57**: 677–701.
- Planchon, S., Gaillardmartinie, B., Dordetfrisoni, E., Bellonfontaine, M., Leroy, S., Labadie, J., *et al.* (2006) Formation of biofilm by *Staphylococcus xylosus*. *Int J Food Microbiol* **109**: 88–96.
- Raafat, D., and Sahl, H.G. (2010) Chitosan and its antimicrobial potential – a critical literature survey. *Microb Biotechnol* **2**: 186–201.
- Rumi, M.V., Huguet, M.J., Bentancor, A.B., and Gentilini, E.R. (2013) The *icaA* gene in staphylococci from bovine mastitis. *J Infect Dev Countr* **7**: 556–560.
- Sakemi, Y., Tamura, Y., and Hagiwara, K. (2011) Interleukin-6 in quarter milk as a further prediction marker for bovine subclinical mastitis. *J Dairy Res* **78**: 118–121.
- Schipper, N.G., Varum, K.M., and Artursson, P. (1996) Chitosans as absorption enhancers for poorly absorbable drugs. 1: influence of molecular weight and degree of acetylation on drug transport across human intestinal epithelial (Caco-2) cells. *Pharm Res-Dordr* **13**: 1686–1692.
- Tan, X., Liu, L., Liu, S., Yang, D., Liu, Y., Yang, S., *et al.* (2014) Genome of *Staphylococcus xylosus* and comparison with *S. aureus* and *S. epidermidis*. *J Genet Genomics* **41**: 413–416.
- Wang, J., Peng, H., Kong, J., Zhao, T., Zhang, S., and Cao, X. (2018) Pharmacokinetic profile of ceftiofur hydrochloride injection in lactating holstein dairy cows. *J Vet Pharmacol Ther* **41**: 301–306.
- Xie, T., Liao, Z.L., Lei, H., Fang, X., Wang, J., and Zhong, Q.P. (2017) Antibacterial activity of food-grade chitosan against *Vibrio parahaemolyticus* biofilms. *Microb Pathogenesis* **110**: 291–297.
- Xu, C.-G., Yang, Y.-B., Zhou, Y.-H., Hao, M.-Q., Ren, Y.-Z., Wang, X.-T., *et al.* (2017) Comparative proteomic analysis provides insight into the key proteins as possible targets involved in aspirin inhibiting biofilm formation of *Staphylococcus xylosus*. *Front Pharmacol* **8**: 543.
- Zhang, L., Parsons, D.L., Navarre, C., and Kompella, U.B. (2002) Development and in-vitro evaluation of sustained release poloxamer 407 (P407) gel formulations of ceftiofur. *J Control Release* **85**: 73–81.